IEEE Access
Multidisciplinary | Rapid Review | Open Access Journal

Received July 11, 2019, accepted July 19, 2019, date of publication July 24, 2019, date of current version August 8, 2019.

Digital Object Identifier 10.1109/ACCESS.2019.2930895

Mutually Coupled Switched Reluctance Motor: Fundamentals, Control, Modeling, State of the Art Review and Future Trends

PETER AZER, (Student Member, IEEE), BERKER BILGIN, (Senior Member, IEEE), AND ALI EMADI, (Fellow, IEEE)

McMaster Institute for Automotive Research and Technology, McMaster University, Hamilton, ON L8P 0A6, Canada

Corresponding author: Peter Azer (eliap@mcmaster.ca)

This work was supported in part by the Canada Excellence Research Chairs (CERC) Program.

ABSTRACT Switched reluctance motor (SRM) is gaining more interest in the last decades due to its simple and robust structure. SRMs are classified into conventional SRMs (CSRMs) and mutually coupled SRMs (MCSRMs). CSRMs are based on single-phase excitation and torque is generated by the variation of self-inductance with rotor position. MCSRMs are based on multi-phase excitation and torque is produced by the rate of change of both self- and mutual inductances. MCSRM has the advantages of using the standard voltage source inverter at balanced current operation, when the sum of the phase currents is zero, while CSRM requires an asymmetrical converter. This paper presents the state-of-the-art review of MCSRMs, including operating concept, winding, and pole configurations, control methods by using different current waveforms, performance comparison of MCSRM configurations, modeling methods, and future work for improving MCSRM performance.

INDEX TERMS Double/single layer winding, motor control, mutually coupled switched reluctance motor, modeling, short/full pitched winding, state-of-the-art review.

I. INTRODUCTION

Switched reluctance motors (SRMs) are characterized by their simple and robust structure among other electric motors due to the absence of coils or permanent magnets on the rotor. However, high torque ripples and acoustic noise can be factors limiting their application. In the last few decades, SRMs have been gaining more attention due to the advancements in power electronics which enable complicated control strategies to improve motor performance [1], [2].

Conventional switched reluctance motor (CSRM) which is also known as the traditional SRM is firstly introduced by Ray, Davis and Lawrenson in 1979 and 1980 by using single phase excitation as an extension of stepper motors [3], [4]. Torque production in CSRM is due to the tendency of the magnetic flux generated by the excited phase to have a minimum reluctance path. As a result, the rotor position changes until the rotor pole and the excited stator pole are aligned achieving the minimum reluctance path [3].

The associate editor coordinating the review of this manuscript and approving it for publication was Ton Do.

Due to the single phase excitation and the winding configuration of CSRM, torque is generated by the rate of change of self inductance independent of the direction of current [5]. In CSRM, commutation happens when two phases have current at the same time. This overlapping occurs when one phase is excited while the other phase is not fully demagnetized. The mutual coupling during commutation is usually negligible. This is because the winding configuration in SRM minimizes the mutual flux path and the phase currents are small during commutation [6].

Mutually coupled switched reluctance motor (MCSRM) is first proposed by B.C. Mecrow in 1993 and 1996. In MCSRM, at least two phases are excited at the same time [7], [8]. The torque production principles are similar to CSRM of achieving the minimum reluctance path. The difference for the MCSRM is that multiple phases are excited at the same time; hence, torque is generated by the variation of self and mutual inductances with rotor position [9], [10]. Along with the multi-phase excitation, the winding configuration in MCSRM enhances the mutual coupling between phases. Multi-phase excitation has also been introduced for CSRM in [11]. In this paper, we will focus on

MCSRMs and multi-phase excitation in CSRM will not be discussed.

It has been claimed that, MCSRM has better performance than CSRM regarding vibration and acoustic noise. Authors in [12] have shown that the 3-phase 6/4 MCSRM has radial forces half that of 6/4 CSRM for the same output torque. In [13], it was demonstrated that the 3-phase 12/8 MCSRM has lower vibration and lower sound pressure level (SPL) than the the 3-phase 12/8 CSRM, when both motors have the same geometry and are supplied by the same sinusoidal current.

The standard current waveform of CSRM is unipolar rectangular waveform. In order to improve the performance of a CSRM, advanced control techniques, such as current profile shaping, are applied to reduce the torque ripple and acoustic noise [14]–[17]. Current waveform of MCSRM can be unipolar rectangular waveform, bipolar rectangular waveform or sine waveform [8], [18], [19]. MCSRM can have a double layer short pitched, single layer short pitched or full pitched winding configuration.

Due to its salient-pole stator and rotor construction, SRM is named as a doubly-salient reluctance motor [8], [19]. The inductance or flux linkage models are dependent on the rotor position and also the level of excitation current, due to non-linear characteristics of the core material. Therefore, look-up table (LUT) based methods are commonly utilized for the modeling of both motors.

Previous review papers focus on either the control [20] or design of CSRMs [21]. A comprehensive review paper on MCSRMs is not available in the literature. Therefore, this paper presents a detailed review of MCSRMs in terms of pole configurations, winding configurations, control methods, and the converters. A performance comparison for different MCSRM control methods and configurations is also provided. The paper also includes a comparative study of the modeling methods with a detailed explanation for the most accurate one.

The rest of the paper is organized as follows: Section II presents the operating concept including the possible pole and winding configurations. Section III summarizes different control methods followed by a performance comparison for those control methods and MCSRM configurations. Modeling of MCSRM is shown in Section IV. Future work to improve MCSRM performance is discussed in Section V. Finally, Section VI presents the conclusions of the paper.

II. OPERATING CONCEPT

Torque production in SRM is due to the tendency of the generated magnetic flux to have a minimum reluctance path, which in return rotates the rotor until the rotor pole becomes aligned with the excited stator pole, maximizing the inductance of the excited phase.

Considering a single phase SRM shown in Fig. 1(a) and for a linear magnetic system shown in Fig. 1(b) (i.e., inductance does not change with current) half of the input electrical energy is stored in the magnetic circuit, which is known as the

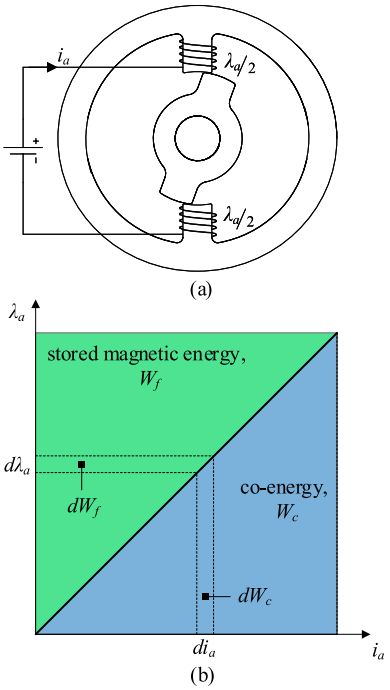

FIGURE 1. (a) single phase SRM, (b) flux linkage versus current for a linear magnetic system.

field energy. The lower half is converted to mechanical energy and it is responsible for torque production. It is known as the co-energy. Equation (1) describes the energy conversion dynamics:

$$ei_a dt = dW_f + T_e d\theta \tag{1}$$

where i_a is phase a current, W_f is the field energy transferred between the source and the magnetic circuit, and is equivalent to reactive power, and T_e is the electromagnetic torque responsible for angular displacement, $d\theta$. e is the induced emf and its magnitude is expressed by Faraday's law:

$$e = \frac{d\lambda_a}{dt} \tag{2}$$

where λ_a is phase a flux linkage. Using (2), (1) can be formulated as:

$$i_a d\lambda_a = dW_f + T_e d\theta \tag{3}$$

From Fig. 1(b), the summation of field energy and co-energy is:

$$\lambda_a i_a = W_c + W_f \tag{4}$$

$$d(\lambda_a i_a) = \lambda_a di_a + i_a d\lambda_a = dW_c + dW_f \tag{5}$$

From (3) and (5), co-energy can be formulated as:

$$dW_c = \lambda_a di_a + T_e d\theta \tag{6}$$

Co-energy is a function of current and rotor position. Hence, the partial derivatives of co-energy is equal to:

$$dW_c = \frac{\partial W_c}{\partial \theta} \mathrm{d}\theta \Big|_{i_a = const} + \frac{\partial W_c}{\partial i_a} \mathrm{d}i_a \Big|_{\theta = const} \tag{7}$$

Comparing (6) and (7), flux linkage and torque expressions can be calculated as:

$$\lambda_a = \left.\frac{\partial W_c}{\partial i_a}\right|_{\theta=const}, \; T_e = \left.\frac{\partial W_c}{\partial \theta}\right|_{i_a=const} \tag{8}$$

For a linear magnetic circuit shown in Fig. 1(b), co-energy is half of the input electrical energy:

$$W_c = \frac{1}{2}\lambda_a i_a \tag{9}$$

Assuming two phases are excited simultaneously (phases a and b), co-energy can be expressed as:

$$W_c = \frac{1}{2}\lambda_a(\theta, i_a, i_b)\, i_a + \frac{1}{2}\lambda_b(\theta, i_a, i_b)\, i_b \tag{10}$$

where i_b and λ_b are phase b current and flux linkage, respectively. Flux linkages include self and mutual inductances and are functions of phase currents and rotor position:

$$\lambda_a(\theta, i_a, i_b) = i_a L_a + i_b M_{ab}, \tag{11a}$$
$$\lambda_b(\theta, i_a, i_b) = i_b L_b + i_a M_{ab} \tag{11b}$$

where L_a is phase a self inductance, L_b is phase b self inductance and M_{ab} is the mutual inductance between phases a and b. Substituting (11) into (10) results in:

$$W_c = \frac{1}{2}(L_a i_a^2 + L_b i_b^2 + 2 i_a i_b M_{ab}) \tag{12}$$

Therefore, electromagnetic torque equals to:

$$T_e = \left.\frac{\partial W_c}{\partial \theta}\right|_{i=const} = \frac{1}{2} i_a^2 \frac{dL_a}{d\theta} + \frac{1}{2} i_b^2 \frac{dL_b}{d\theta} + i_a i_b \frac{dM_{ab}}{d\theta} \tag{13}$$

Similarly, for 3-phase excitation (phases a, b, and c) the torque equation is expressed as:

$$T_e = \frac{1}{2} i_a^2 \frac{dL_a}{d\theta} + \frac{1}{2} i_b^2 \frac{dL_b}{d\theta} + \frac{1}{2} i_c^2 \frac{dL_c}{d\theta} + i_a i_b \frac{dM_{ab}}{d\theta} + i_a i_c \frac{dM_{ac}}{d\theta} + i_b i_c \frac{dM_{bc}}{d\theta} \tag{14}$$

where L_c is phase c self inductance, M_{ac} is the mutual inductance between phases a and c and M_{bc} is the mutual inductance between phases b and c. For CSRM where mutual coupling between phases is ignored, $M_{ab} = M_{bc} = M_{ac} = 0$. Based on (14), torque developed due to self inductance is dependent on the slope of the inductance profile and independent of the direction of current, similar to CSRM. While torque developed due to mutual coupling is dependent on both the direction of current and slope of the inductance.

A. POLE CONFIGURATION

Number of stator and rotor poles in MCSRM is selected to achieve balanced operation for a given number of phases. This means that stator poles which belong to the same phase should have the same electrical angle at any rotor position. In light of that, pole configuration and phase number in SRM are expressed by (15).

$$LCM(N_s, N_r) = mN_r \tag{15}$$

where LCM represents the least common multiple operator, N_s is the number of stator poles, N_r is the number of rotor poles, and m is the number of phases. It is worth mentioning that number of stator poles per phase is always an integer number for SRMs.

B. WINDING CONFIGURATION

Concentrated winding is widely utilized in SRMs, where the coils are concentrated in one slot. As CSRM has single phase excitation, the concentrated winding provides the highest magnetomotive force (MMF) to maximize the generated electromagnetic torque [7], [22]–[25].

1) SINGLE LAYER SHORT PITCHED SRM [13], [18], [19], [26], [27]

A stator slot in single layer windings has one phase coil and it is not shared by other phase coils. So, the number of coils is half of the number of stator poles. The angular displacement between poles is 180° electrical, and it is called pole span or pole pitch. If the coil span is less than the pole span (180° electrical), then it is called a short pitched winding as shown in Fig. 2(a).

Single layer short pitched winding can be CSRM or MCSRM. In CSRM, each two consequent stator poles of the same phase has different polarities. These poles create a single flux path. Therefore, the magnetic flux path in CSRM is within the stator poles of the excited phase only and negligible flux flows through the stator poles of an unexcited phase. This can be seen in Fig. 2(a). The consequent stator poles of phase a have different polarities of North (N) and South (S). All flux paths are through the excited phase a poles and there is almost no flux paths within the poles of the other phases. This is why the mutual coupling in CSRM can be ignored.

In MCSRM, to enhance the mutual coupling between phases, the stator poles of the same phase have the same polarity. Thus, flux generated by one phase have flux paths through the poles of the other phases. As it can be seen from Fig. 2(b), the flux generated by the excited phase a have flux paths through other phases which creates mutual coupling between phases.

Equation (15) can result in odd number of stator poles, for instance, 9/12 3-phase SRM. The odd number of stator poles is only valid for MCSRM as CSRM requires even number of stator poles [5], so that each two consequent stator poles provide one flux path.

2) DOUBLE LAYER SHORT PITCHED SRM [13], [19], [26]–[29]

The difference between the double layer short pitched winding with that of single layer one is that two coils of different phases share the same slot in the double layer winding. Thus, the number of coils is equal to the number of stator poles. Similar to single layer short pitched winding, double layer short pitched winding can be CSRM or MCSRM.

Fig. 2(c) and Fig. 2(d) show the winding diagrams for double layer short pitched 12/8 CSRM (DL-SP-CSRM) and

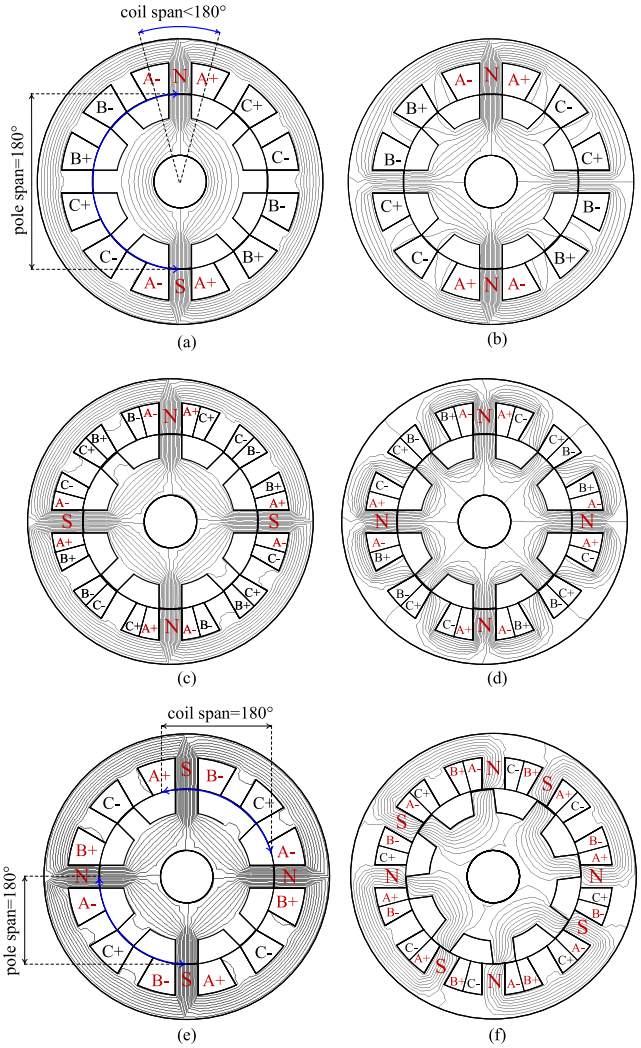

FIGURE 2. Winding configuration of 3-phase 12/8 SRM and flux distribution when phase *a* is excited (a) single layer short pitched CSRM, (b) single layer short pitched MCSRM, (c) double layer short pitched CSRM, (d) double layer short pitched MCSRM. When phases *a* and *b* are excited (e) single layer full pitched MCSRM, (f) double layer fractional pitched MCSRM.

MCSRM (DL-SP-MCSRM), respectively. The flux paths are also shown when phase *a* is excited. It can be observed that the polarity of the coils define whether the motor is a CSRM or MCSRM. As shown in Fig. 2(d), the coils of the same phase in MCSRM have the same polarity. Therefore, the magnetic path is through the poles of the other phases, enhancing the mutual coupling. As shown in Fig. 2(c), the coils of the same phase in CSRM have opposite poles. Therefore, the flux paths only use the stator poles of phase *a*.

3) SINGLE LAYER FULL PITCHED SRM [7]–[10], [19], [27], [30]–[32]

In full pitched winding, the coil span is equal to pole span (180° electrical). Fig. 2(e) shows single layer full pitched 12/8 MCSRM (SL-FP-MCSRM). In a full pitched configuration, single phase excitation is not enough to magnetize any stator pole. Therefore, at least two phases should be excited simultaneously. This is why single layer full pitched winding can only work as a MCSRM.

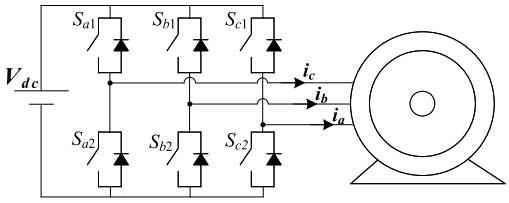

FIGURE 3. 2-level voltage source inverter for dependent phase current control.

4) DOUBLE LAYER FRACTIONAL PITCHED SRM [33]

The fractional pitched winding is similar to the short pitched winding but with different coil span as shown in Fig. 2(f). This winding configuration is not commonly applied. The single layer full pitch winding that was described earlier, provides constant self inductance when applied to MCSRM. Hence, torque production relies on the variation of the mutual inductance [7]. The double layer fractional pitched winding utilizes self and mutual inductances in torque generation [33].

III. CONTROL

In electric motors, the motor speed is regulated by controlling the electromagnetic torque, which is controlled through the phase currents. Current control in MCSRMs can be classified into dependent phase current control and independent phase current control.

A. DEPENDENT PHASE CURRENT CONTROL

Dependent phase current control is referred to the case when the sum of phase currents at any time instant is zero. In this control strategy, MCSRM can be considered as an AC motor where the standard voltage source inverter (VSI) shown in Fig. 3 can be used. Phase current can be any type of waveform, such as sinusoidal or bipolar rectangular (alternating between positive and negative half cycles) as long as the phase currents add up to zero. Thus, MCSRM can replace the AC motors in different applications such as electric vehicles.

1) SINUSOIDAL CURRENT EXCITATION [10], [13], [19], [26], [27], [34], [35]

Fig. 4(a) shows 3-phase sinusoidal currents, which is the most common way for motor control. The system parameters for sinusoidal excitation can be calculated as [36]:

$$T_{avg} = \frac{3}{2}p(\lambda_d i_q - \lambda_q i_d) \tag{16}$$

$$v_d = i_d R - \lambda_q w \tag{17}$$

$$v_q = i_q R + \lambda_d w \tag{18}$$

$$P = \frac{3}{2}(v_d i_d + v_q i_q) \tag{19}$$

$$Q = \frac{3}{2}(v_q i_d - v_d i_q) \tag{20}$$

$$cos(\phi) = \frac{P}{\sqrt{P^2 + Q^2}} \tag{21}$$

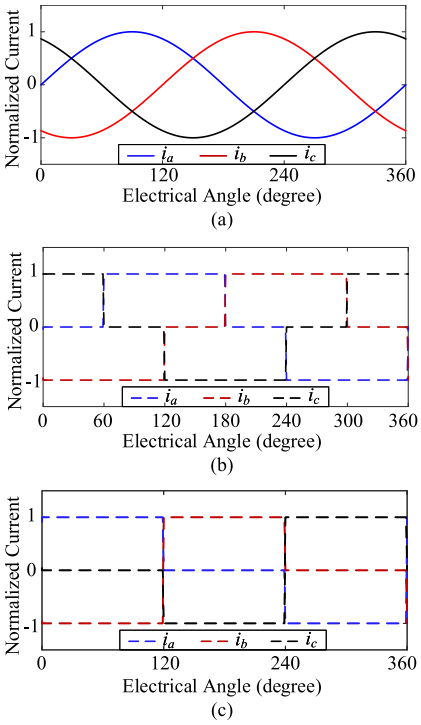

FIGURE 4. Dependent phase current control (a) Sinusoidal current excitation, symmetric bipolar current (b) 60° zero current +120° positive current +60° zero current +120° negative current [7]–[9], [26], [35], [37]–[39], (c) 120° positive current +120° zero current +120° negative current [18], [26], [33].

where T_{avg} is the output average torque, w is the electrical angular frequency, p is the number of pole pairs and is equal to half of the number of rotor poles. λ_d and λ_q are dq components of phase flux linkage, v_d and v_q are the dq components of the phase voltage, and i_d and i_q are the dq components of the phase current. R is the phase resistance, and P and Q are active and reactive power, respectively. $cos(\phi)$ is the power factor of the three-phase load.

Equations (16) to (21) describe the average torque calculation, active power, reactive power, and power factor. Sinusoidal current control is the only control method that provides these direct formulas for system parameters calculation, which is an advantage. Another advantage of the sinusoidal current excitation is that the vector control (dq-current control) can be applied with space vector modulation (SVM) or sinusoidal pulse width modulation (SPWM) like in AC motors. Thus, there is no need to use hysteresis current controller (HCC) which is commonly used in CSRMs. HCC has the advantages of fast dynamic response, maximum current limitation, and simple implementation. Since the sum of phase currents is zero in a balanced 3-phase system (referred as inter-phase dependency), a major drawback of HCC is the high switching frequency operation as each phase is controlled separately without the coordination with other phases [40]–[42]. The inter-phase dependency is considered in SVM since the 3-phase currents are controlled by one vector representing the line voltage.

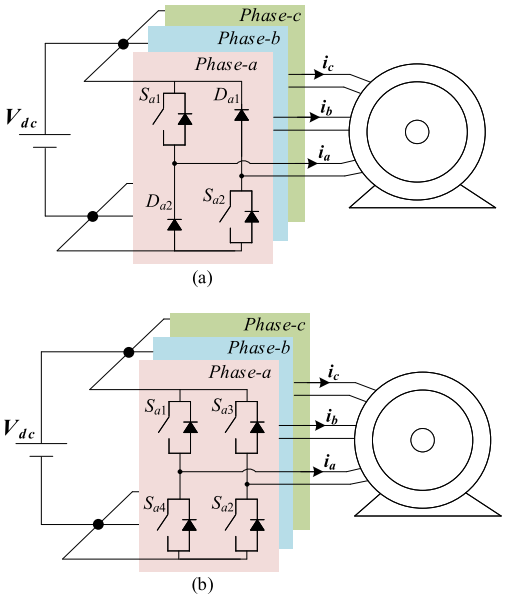

FIGURE 5. Converters used for independent phase current control (a) Asymmetric half-bridge converter for unipolar excitation, (b) Symmetric full-bridge converter for bipolar excitation.

2) SYMMETRIC BIPOLAR CURRENT EXCITATION [7]–[9], [18], [26], [28], [33], [35], [37]

Bipolar current excitation is when the current waveform alternates between the positive and negative half cycles. Fig. 4(b) and Fig. 4(c) show two rectangular current waveforms where the sum of the instantaneous values of the phase currents is zero.

Usually two phases are excited simultaneously; one phase current has positive magnitude and the other phase current has the same magnitude, but with negative polarity. The phase shift between phase currents is $360/m$ (m is the number of phases), which is 120° electrical for a 3-phase MCSRM. HCC is usually used in symmetric bipolar excitation to regulate the current.

B. INDEPENDENT PHASE CURRENT CONTROL

In the independent phase current control, the sum of the instantaneous values of the phase currents is not zero and, hence, the standard VSI cannot be used. If phase currents are unipolar, then an asymmetric half bridge converter is used to control each phase separately as shown in Fig. 5(a) [1], [2]. If phase currents are bipolar, then a single-phase full bridge inverter is used for each phase as shown in Fig. 5(b) [43]. As phase currents are not sinusoidal, SVM and SPWM cannot be used and HCC is usually utilized to control the current.

1) UNIPOLAR CURRENT EXCITATION

Unipolar current excitation in MCSRM is similar to CSRM, but the conduction period is increased to provide overlapping between phase currents. For instance, conduction period for a 3-phase MCSRM is larger than 120° electrical. Fig. 6(a) shows unipolar current excitation for 180° electrical conduction period [18], [37] and Fig. 6(b) shows

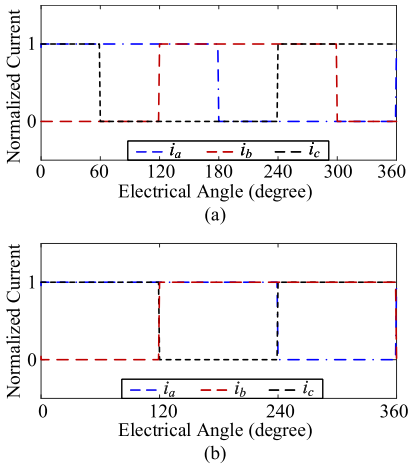

FIGURE 6. Independent phase current control: Unipolar current excitation of (a) 180° conduction period (180° positive current +180° zero current), (b) 240° conduction period (240° positive current +120° zero current).

unipolar current excitation for 240° electrical conduction period [7]–[9], [37], [44], [45] for a 3-phase MCSRM.

2) NON-SYMMETRIC BIPOLAR CURRENT EXCITATION

Non-symmetric bipolar phase current is when the positive and negative current half cycles are not identical. Non-symmetric bipolar current excitation is introduced in [18], [26], [46], and [47] to increase the torque generated from mutual inductance.

Figs. 7(a) and 7(b) show current waveforms for a 3-phase MCSRM for 180° [18], [46], [47] and 360° [26] electrical conduction periods, respectively.

3) SYMMETRIC BIPOLAR CURRENT EXCITATION [7], [8], [37]

The conduction period is the main difference between the symmetric bipolar excitation for independent phase current control and for dependent phase current control discussed in Section III-A.2. The symmetric current in dependent phase control has a conduction period of 240° electrical (see Fig. 4(b)), while the bipolar current for independent control has a conduction period of 360° electrical as shown in Fig. 7(c).

It should be noted that the currents shown in Figs. 4, 6, and 7 (except for the sinusoidal current) are applicable only at low speed operation, generally when the motor speed is lower than the base speed. When the motor speed is higher than the base speed, the phase current has a different waveform at different operating speeds. For instance, Fig. 8 shows unipolar current excitation waveforms at low speed and high speed operation. It can be seen from Fig. 8 that, at low speed, the phase current waveform reaches the reference value where switching action takes place. This is defined as current chopping control (CCC) which results in a phase current waveform close to the rectangular waveform. At high speed (i.e., when motor speed exceeds the base speed), the induced emf is higher than the DC link voltage. Thus, phase current might not reach the reference value.

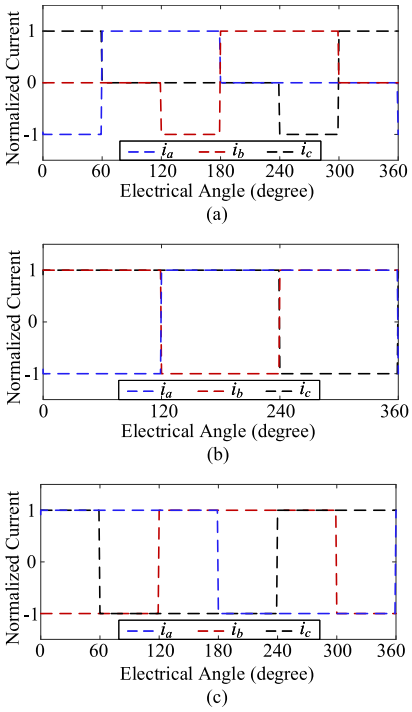

FIGURE 7. Independent phase current control: Non-symmetric bipolar current excitation of (a) 180° conduction period (60° negative current +120° positive current +180° zero current), (b) 360° conduction period (120° negative current +240° positive current), (c) symmetric bipolar current excitation for 360° conduction period (180° positive current +180° negative current).

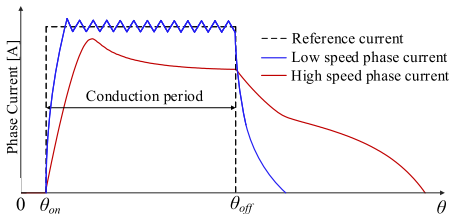

FIGURE 8. Unipolar current excitation at low speed operation where current control is applicable and high speed operation where current control is not applicable.

This is defined as the single pulse control where a duty ratio of one is applied to the switching device (phase voltage is equal to the DC link voltage). When the rotor position reaches θ_{off}, the duty cycle is zero (phase voltage is equal to the negative DC link voltage). At high speed operation, when current control is not available, different motor speeds result in different values of induced emf, which in turn creates different phase current waveforms. The same issue also exists in CSRMs.

Sinusoidal phase currents do not have the high rate-of-change as in the rectangular waveforms shown in Figs. 4, 6, and 7. Therefore, the current waveform can be maintained as sinusoidal or close to sinusoidal even at high speeds [48], [49]. This is another advantage for sinusoidal excitation.

C. PERFORMANCE COMPARISON

In this section, a performance comparison for different winding configurations for a 3-phase 12/8 MCSRM with different

TABLE 1. Motor specifications.

Number of stator poles	12	Number of turns/phase	132
Number of rotor poles	8	Stator outer diameter	90
Phase number	3	Rotor outer diameter	53
Rated RMS current (A)	10	Rotor inner diameter	31.4
Current density (A_{rms}/mm^2)	5.68	Air-gap length (mm)	0.5
Active length (mm)	60		

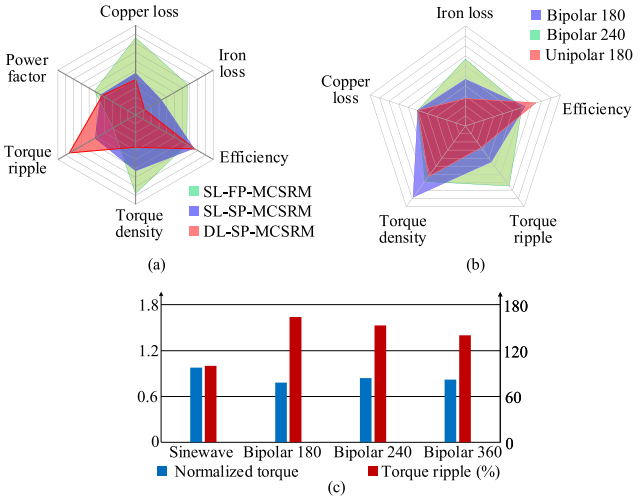

FIGURE 9. 12/8 MCSRM performance comparison (at the rated current) for (a) different winding configurations with 3-phase sinusoidal current excitation, (b) different control methods for SL-SP-MCSRM, (c) different control methods for DL-SP-MCSRM.

control methods is presented. The motor dimensions and parameters are shown in Table 1 [18], [19], [26].

1) SINUSOIDAL CURRENT CONTROL [19]

The performance of the 3-phase 12/8 MCSRM controlled by sinusoidal current excitation at the rated phase current is analyzed for three winding configurations: full pitched, double layer short pitched, and single layer short pitched. Fig. 9(a) presents the performance comparison, and it includes torque density, the maximum achievable base speed with the same DC link voltage, power factor and iron loss at that base speed, copper loss, maximum achievable efficiency, and torque ripple.

The SL-FP-MCSRM has the highest copper loss because it has the largest end winding length compared to other winding configurations. The SL-SP-MCSRM has 2 coils per phase, and the DL-SP-MCSRM has 4 coils per phase. In order to have equal number of turns per phase in the single and double layer configurations, SL-SP-MCSRM has twice the number of turns per coil which results in higher mean length per turn compared to the DL-SP-MCSRM. Therefore, SL-SP-MCSRM has a slightly higher copper length than DL-SP-MCSRM and, hence, higher copper loss.

SL-FP-MCSRM has the highest variation in stator and rotor flux density compared to other winding configurations, so it has the highest iron loss [19]. DL-SP-MCSRM has the lowest iron loss. The efficiency of DL-SP-MCSRM is slightly higher than SL-SP-MCSRM. As the copper loss is more significant than iron loss in the low-power 12/8 MCSRM used in this comparison. Since, SL-FP-MCSRM has the highest copper loss, it has the lowest efficiency.

Single layer winding configurations (SL-FP-MCSRM and SL-SP-MCSRM) have double the number of turns per coil in comparison with the double layer winding (DL-SP-MCSRM), and they can generate higher level of saturation. Among the single layer winding configurations, SL-FP-MCSRM can generate higher saturation for the same MMF compared to SL-SP-MCSRM. With saturation, the effective inductance and the required reactive power decrease. So the machine can achieve higher power factor. Therefore, SL-FP-MCSRM has the highest power factor and DL-SP-MCSRM has the lowest power factor.

The difference between the torque performances with sinusoidal current control can be analyzed based on the motor inductances. The electromagnetic torque in (16) can be expressed in terms of inductance components:

$$T_{avg} = \frac{3}{2} p(L_d - L_q) I_d I_q \tag{22}$$

where L_d and L_q are dq inductances, and I_d and I_q are dq currents. $(L_d - L_q)$ is maximum for SL-FP-MCSRM and minimum for DL-SP-MCSRM. Therefore, SL-FP-MCSRM and DL-SP-MCSRM have the highest and lowest torque density, respectively. Fig. 9(a) also shows that DL-SP-MCSRM and SL-FP-MCSRM have the highest and lowest torque ripple, respectively.

2) SL-SP-MCSRM [18]

The 3-phase 12/8 SL-SP-MCSRM can also be controlled by unipolar current excitation of 180° conduction period (Section III-B.1), bipolar current excitation of 180° conduction period (Section III-B.2), and bipolar current excitation of 240° conduction period (Section III-A.2). Fig. 9(b) compares the performance of these excitations. The three excitation currents have the same RMS value and they are applied to the same winding configuration with the same resistance. Hence, they generate the same copper loss. The bipolar current excitations (180° and 240° conduction periods) have higher iron loss than unipolar current excitation due to the change in the polarity of the magnetic flux density.

The torque components generated by self and mutual inductances differ for each current excitation. The torque component by self inductance depends on the variation of the self inductance with rotor position and the torque component by mutual coupling (14) depends on both the direction of the phase current and the slope of mutual inductance profile. The generated electromagnetic torque is the summation of these torque components. Fig. 9(b) shows that bipolar current excitation of 180° conduction period and unipolar current excitation of 180° conduction period have the highest and lowest total torque, respectively. Fig. 9(b) also shows that the bipolar current excitation of 240° conduction period and the unipolar current excitation of 180° conduction period has

the highest and lowest torque ripples, respectively. As the three current excitations have the same copper loss, the efficiency difference at the given rotor speed depends on the iron loss. Thus, unipolar current excitation of 180° and bipolar current excitation of 240° have the maximum and minimum efficiencies, respectively.

3) DL-SP-MCSRM [26]

The 3-phase 12/8 DL-SP-MCSRM can be controlled by sinusoidal excitation, bipolar current excitation of 180° conduction period (Section III-B.2), bipolar current excitation of 240° conduction period (Section III-A.2), and bipolar current excitation of 360° conduction period (Section III-B.3). Performance comparison presented in Fig. 9(c) is based on average torque and torque ripple. Although the bipolar current excitation of 360° conduction period generates the highest torque component by mutual coupling [26], it also generates negative torque by the self inductance. This results in lower total torque as compared to the sinusoidal excitation. As it can be seen from Fig. 9(c), sinusoidal excitation achieves balanced self and mutual torque components ending up with higher total torque than the other bipolar current excitation types. The sinusoidal excitation has the minimum torque ripples as it provides smoother change in the current waveform. The other bipolar rectangular currents have a higher rate-of-change of current.

IV. MODELING

Modeling establishes a relationship between the phase currents, phase flux linkages (or inductances), and rotor position, which is necessary to analyze the performance of the motor. Only the modeling methods that consider mutual coupling are discussed in this section. Modeling methods can be either a derivative model or an integral model. In the derivative model, the phase current is considered as a state variable and other parameters such as torque and phase flux linkage are a function of the phase current which is calculated as:

$$i_{phase} = \frac{v - \dfrac{d\lambda_{phase}}{dt}}{R} \tag{23}$$

where λ_{phase}, i_{phase}, and v_{phase} are the phase flux linkage, phase current, and phase voltage, respectively. In the integral model, the phase flux linkage is considered as a state variable. Phase current and torque are a function of the phase flux linkage which is calculated as:

$$\lambda_{phase}(i, \theta) = \int (v_{phase} - i_{phase}R)dt \tag{24}$$

The integral model is more accurate than the derivative model, as the flux linkage derivative amplifies the noise in the model [50]. For instance, if there is a 5^{th} order harmonic noise, its derivative has a magnitude which equals to the magnitude of this 5^{th} order harmonic multiplied by the angular frequency and a constant of five. Modeling methods can be used in optiimzing motor design through simulating motor performance at different conditions.

A. ANALYTICAL METHODS

Analytical modeling methods are based on non-linear equations to describe the non-linear relationship between the phase current, phase flux linkage, and rotor position.

1) INDUCTANCE MODELING

The self and mutual inductance profiles are expressed by Fourier series in this method [51]–[58]. If the first three harmonic orders are considered, the self inductance is expressed as:

$$L(i, \theta) = \sum_{n=0}^{\infty} L_n(i)cos(n\theta) \tag{25}$$

$$L(i, \theta) = L_0(i) + L_1(i)cos(n\theta) + L_2(i)cos(2n\theta) \tag{26}$$

where $L_0(i)$, $L_1(i)$ and $L_2(i)$ are Fourier coefficients of the DC value, first order and second order harmonics. In order to solve $L_0(i)$, $L_1(i)$ and $L_2(i)$, the inductance values at three different rotor positions are calculated by finite element analysis (FEA) or measured from experiments for single phase excitation. For more accurate modeling of self inductance, the first five harmonic orders can be considered instead of three. In this case, five rotor positions will be required to solve for the five Fourier coefficients [59], [60].

Similarly, the mutual coupling of the excited phase on the unexcited phase can be expanded by Fourier series as [52]:

$$M(i, \theta) = \sum_{n=0}^{\infty} M_n(i)cos(n\theta) \tag{27}$$

where $M_n(i)$ represents the Fourier series coefficients. For 2-phase excitation, the mutual inductance is a function of the two phase currents [51], [61]:

$$M(i_x, i_y, \theta) = \sum_{n=0}^{\infty} M_n(i_x, i_y)cos(n\theta) \tag{28}$$

where i_x and i_y are the currents of the excited phases. Solving (28) is complicated as it is a function of two phase currents unlike the case for the self inductance. Authors in [62] mentioned that solving (28) requires at least 4 rotor positions and 10 steps of each phase current, resulting in 400 measurements. This explains why (28) was mentioned in [51] and [61] without solving it. Equation (28) is for 2-phase excitation, thus, the complexity of the inductance model increases as the number of excited phases increases. As a result, it can be concluded that the inductance model can successfully model the self inductance in linear and saturation regions like the case in CSRMs where single phase excitation dominates. However, it is more complicated to model the MCSRMs using the inductance model.

2) MAGNETIC CIRCUIT MODELING

The least common analytical modeling method for MCSRMs is the magnetic circuit modeling due to its high level of complexity. The equivalent magnetic circuit of SRM can be modeled with a number of reluctance elements. There is no

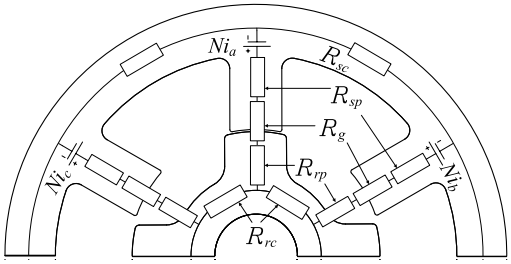

FIGURE 10. Magnetic circuit model for 3-phase 6/4 SRM.

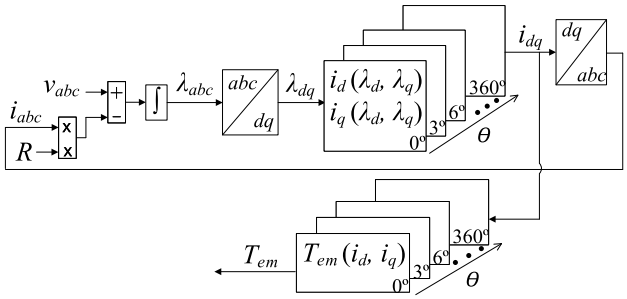

FIGURE 11. Dynamic model of a 3-phase MCSRM for dependent phase current control.

standard way to model the equivalent magnetic circuit like the case in inductance modeling. Several approaches have been proposed to increase the model accuracy at the expense of model complexity and simulation time [30], [63]–[65]. It can be generalized that there are five main reluctances describing stator core R_{sc}, rotor core R_{rc}, stator pole R_{sp}, rotor pole R_{rp} and air gap R_g as shown in Fig. 10.

It is worth mentioning that magnetic circuit models which include the mutual coupling effect are either for CSRMs to model the mutual coupling during commutation [64], [65] or for MCSRMs with two phases of equal current excitation [30], [63] where the excited phases have the same current waveform without phase shift. Authors in [66] and [67] show that the mutual inductance change with current in CSRM is negligible even during saturation. This simplifies the mutual coupling model as an inductance which varies only with rotor position. Thus, models in [65] and [64] cannot be used for MCSRMs modeling. In MCSRM, the 2-phase equal current excitation is equivalent to single phase excitation [9] as the two phases carry the same current, which also simplifies the modeling of the mutual coupling. Therefore, the models in [63] and [30] cannot accurately model the mutual coupling if the two excited phases have different current values.

B. LOOK-UP TABLE BASED MODELS

Modeling methods which use LUTs have higher accuracy compared to the analytical models which use empirical formulas. For single phase excitation like the case in CSRMs, a 2D LUT is obtained from FEA or experimentally. This LUT has single phase current and rotor position as inputs, and phase flux linkage as the output, and it can be represented as $\lambda_{phase} = f(i_{phase}, \theta)$. For the integral model, which is less prone to errors and noise amplification as compared to the derivative model, the LUT should be inverted to obtain the phase current from the phase flux linkage: $i_{phase} = f(\lambda_{phase}, \theta)$ [50]. In order to model the instantaneous torque, another 2D LUT is required which expresses the relationship between the phase current, rotor position, and electromagnetic torque: $T_e = f(i_{phase}, \theta)$. For CRSMs, since mutual coupling is negligible, a 2D LUT for one phase can be used to model the operation of the motor. For multi-phase excitation, such as for a 3-phase motor, since mutual coupling cannot be ignored, four 4D LUTs would be needed to describe the relationship between phase currents, phase flux linkages, and torque: $\lambda_{a,b,c} = f(i_a, i_b, i_c, \theta)$ and $T_e = f(i_a, i_b, i_c, \theta)$. The mutual coupling between phases is modeled by considering the total phase flux linkages (λ_{abc}) into account, instead of separately calculating the self and mutual inductance. This increases the accuracy and simplifies the calculations.

1) DEPENDENT PHASE CURRENT MODELING

As discussed in Section III-A, in dependent phase current control, the sum of phase currents is zero at any instant (such as in a balanced 3-phase system). In this case, the LUTs dimension is reduced from 4D to 3D by transforming the system variables from abc stationary frame ($\lambda_{a,b,c} = f(i_a, i_b, i_c, \theta)$) to dq rotating frame ($\lambda_{d,q} = f(i_d, i_q, \theta)$). Reducing the size of the LUTs results in faster simulation time and provides more flexibility in obtaining the inverted LUTs for the integral model. By transforming the stationary frame variables into rotating frame variables, a MCSRM can be modeled similar to an AC motor. The model considers saturation and spatial harmonics by obtaining the flux linkages and the instantaneous torque LUTs as a function of dq currents and rotor position. Spatial harmonics is due to the slotting effect of stator teeth which generates a non-uniform magnetic field. In other words, the stator of MCSRM can be considered as a stator of an AC motor with more salient teeth. A dynamic model of an interior permanent magnet synchronous motor (IPMSM) considering spatial harmonics and saturation was introduced in [68] for a 3-phase 12-slot/8-pole IPMSM. In [69], the same method has been used to model a 3-phase 12/8 MCSRM. Fig. 11 shows the bock diagram of the dynamic models in [68] and [69] for dependent phase current control. First, a range of dq currents that covers two quadratures in the dq frame is defined. The dq currents are then transferred to abc currents for the characterization of the motor in FEA. When d-axis is aligned with phase a at the initial rotor position, abc to dq transformation is known as cosine-based park transformation. In this case, the d-axis is defined as the position where the stator poles of phase a are at the aligned position as shown in Fig. 12(a). If the d-axis is defined to be 90° behind the aligned position for phase a (see Fig. 12(b)), it is referred as sine-based park transformation. In this case, the stator poles of phase a are at the unaligned position at the initial rotor position.

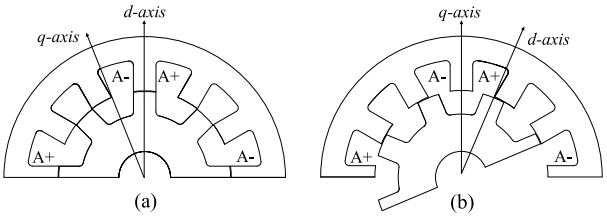

FIGURE 12. Initial rotor position of 12/8 MCSRM when (a) *d*-axis is aligned with phase *a*, (b) *d*-axis is 90° behind phase *a*.

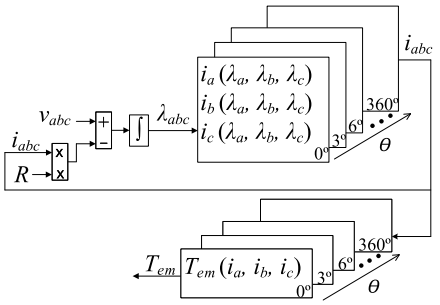

FIGURE 13. Dynamic model of a 3-phase MCSRM for independent phase current control.

The two 3D LUTs $\lambda_d = f(i_d, i_q, \theta)$ and $\lambda_q = f(i_d, i_q, \theta)$ are then inverted to $i_d = f(\lambda_d, \lambda_q, \theta)$ and $i_q = f(\lambda_d, \lambda_q, \theta)$. The 3D LUTs can be considered as multiples of 2D LUTs ($\lambda_d = f(i_d, i_q)$) at different rotor positions. Therefore, the 2D LUTs $\lambda_d = f(i_d, i_q)$ and $\lambda_q = f(i_d, i_q)$ are inverted to $i_d = f(\lambda_d, \lambda_q)$ and $i_q = f(\lambda_d, \lambda_q)$ at each rotor position.

Expressing the *dq* currents as a function of *dq* flux linkages possess some inversion complexity. In order to solve this problem, *gridfit* function [70] from Matlab Central is used in [68]. In [69], *contourc* function from Matlab is used. To our experience, the *gridfit* function in [70] is more flexible than *contourc* for LUTs inversion. For modeling the torque, the 4D LUT ($T_e = f(i_a, i_b, i_c, \theta)$) is reduced to a 3D LUT ($T_e = f(i_d, i_q, \theta)$). An inversion is not needed for the torque LUT.

2) INDEPENDENT PHASE CURRENT MODELING

This type of modeling is applied to independent phase current control, which was discussed in Section III-B. For 2-phase excitation, the same procedures are applied as for the single phase excitation. However, 3D LUTs are obtained instead of 2D LUTs: $\lambda_{a,b} = f(i_a, i_b, \theta)$ and $T_e = f(i_a, i_b, \theta)$. Then, the flux linkage LUTs are inverted to $i_{a,b} = f(\lambda_a, \lambda_b, \theta)$ [71]. Inverting the LUTs is similar to the method described in IV-B.1. The same approach can be applied for any multi-phase excitation. Fig. 13 shows the modeling diagram for independent phase current control.

3) OTHER METHODS

The disadvantage of the LUT based methods is the large number of finite element simulations required to build the LUTs and the complexity in the inversion of LUTs, especially for multi-phase excitation. Authors in [72] tried to reduce FEA steps by using a more coarse phase current range. However, that resulted in considerable errors in the model when compared to FEA results.

Authors in [62] and [73] used feed-forward artificial neural network (FF-ANN) to model the mutual coupling with reduced FEA steps for CSRM and SL-FP-MCSRM, respectively. In [73], FEA results were for 2-phase excitation with keeping one phase current as a constant and assuming linear mutual effect of the constant phase current on the other phase. Results obtained from FEA are applied to ANN through a back-projective training. Keeping one phase current constant value reduced the FEA steps significantly. However, the results did not account for saturation and an experimental validation was not provided [73].

In [62], FF-ANN was used to calculate the mutual flux linkage with 2-phase excitation in CSRM. The data used to train the ANN is obtained from FEA for 2-phase excitation with 25 current cases, which is a relatively low number. No experimental results have been provided to validate the feasibility of this method to model mutual coupling.

Comparing Fig. 2(c) and Fig. 2(e), it can be observed that SL-FP-MCSRM and DL-SP-CSRM have the same flux distribution. As a result, a SL-FP-MCSRM with 2-phase equal current excitation can be considered as a DL-SP-CSRM with single phase excitation. Based on that, authors in [74] developed a model for a 3-phase SL-FP-MCSRM considering the two excited phases as single phase having the same current waveform. Symmetric bipolar current excitation was used with a phase shift of 120° electrical. However, the assumption that the two excited phases have equal current magnitude in symmetric bipolar current excitation is not valid during commutation. This assumption is not valid either at high speed operation when current control is not applicable and current waveforms deviate from the rectangular shape. Thus, the use of this modeling method is limited.

In [32], a dynamic model was introduced for CSRM and SL-FP-MCSRM. Both models use a LUT that describes the relationship between flux per tooth and MMF. The flux per tooth is calculated from the phase flux linkages, and the phase currents are calculated from the MMF. Since both models have the same LUT, the SL-FP-MCSRM model was valid only for 2-phase excitation with equal currents. Therefore, this approach also has limitations in modeling.

In another modeling approach, the authors in [75] and [76] divided each phase of a 12/8 CSRM into two subphases, and each subphase compromises two coils. For instance, phase a is divided into two subphases a_1 and a_2, and both a_1 and a_2 have two coils each. Similarly, phases b and c were divided into b_1, b_2, c_1 and c_2. Two asymmetric half bridge converters were used to supply the 12/8 CSRM, which has four coils per phase, so that one converter is responsible for the subphases a_1, b_1 and c_1, and the other converter is responsible for the subphases a_2, b_2 and c_2. It was claimed that the 12/8 CSRM supplied by two converters instead of one was a new MCSRM, and it was called dual channel MCSRM (DL-MCSRM).

In [75], a dynamic model was introduced for this DL-MCSRM based on decoupling of the subphase flux linkage (λ_{a1}) into self and mutual flux linkages. Since the two subphases a_1 and a_2 have the same current, their self and mutual flux linkage LUTs have a single phase current input. This model is updated in [76], so that LUTs describe the total flux linkage of a_1 and a_2 without decoupling them. This is similar to CSRM modeling. Since the DC-MCSRM is a CSRM supplied by two converters, the models in [75] and [76] cannot be used in MCSRM modeling.

C. MODELING THROUGH CO-SIMULATION

The electromagnetic model of a MCSRM in an FEA software such as JMAG [77] can be used in simulation tools such as Saber [78] or Matlab [79]. This is called co-simulation. It provides the highest accuracy as compared to other methods as it utilizes the FEA model of the motor. However, co-simulation usually requires much longer simulation time, which limits its practicality in the design of a MCSRM drive.

V. FUTURE TRENDS

A. SINUSOIDAL CURRENT CONTROL OF MCSRM

MCSRM with sinusoidal current excitation has significant advantages over other control techniques. Sinusoidal current excitation enables the use of a standard VSI with conventional modulation techniques such as SVM or SPWM without the need for hysteresis control. However, there are some challenges in sinusoidal current excitation. The salient construction of MCSRM stator poles introduces considerable spatial harmonics in the current waveform that cannot be handled by the standard vector control. Spatial harmonics in AC motors is due to the slotting effect and, in most cases, it is negligible. For MCSRM, the salient stator and rotor poles are the main source of reluctance torque and they constitute the main reason for large spatial harmonics. To the authors' knowledge, choosing the optimum values of dq currents to improve the motor performance in terms of torque ripple and efficiency has not been investigated in detail yet for MCSRMs.

B. CURRENT PROFILE SHAPING FOR MCSRM

Current shaping has been widely investigated for CSRMs to reduce the torque ripple and acoustic noise [14]–[17]. Similarly, shaping the phase current waveforms in MCSRM, rather than using the standard current waveforms discussed in Section III, can improve the motor performance significantly. Current shaping can be based on either dependent or independent phase current control. By the time of the writing of this paper, current shaping in MCSRM has not been investigated in the literature.

C. OTHER WINDING CONFIGURATIONS OF MCSRM

As mentioned in Section II-B, CSRM has concentrated winding to maximize the generated MMF for single phase excitation [7], [23]–[25]. As a result, all SRMs (CSRM and MCSRM) have concentrated windings. For multiphase excitation in MCSRM, distributed winding configurations can provide a better performance in terms of torque density and power factor. To the authors' observation, distributed winding configurations for MCSRMs have not been investigated in detail in the literature.

VI. CONCLUSION

In this paper, a comprehensive review of MCSRMs has been presented. MCSRMs are based on multi-phase excitation, which enables the use of a standard VSI in case of balanced current operation. For sinusoidal excitation, the same modulation strategies of AC motors can be used. The commonly used winding configurations for MCSRM are single layer short and full pitched, double layer short pitched, and fractional pitched windings.

The performance of MCSRMs with different winding configurations and different control methods have been presented for a low-power 12/8 MCSRM. For sinusoidal current excitation, the single layer full pitched winding shows better performance in terms of torque density, torque ripple, and power factor. The double layer short pitched winding has the highest efficiency. For single layer short pitched winding, the bipolar phase current of 180° electrical conduction period has the highest torque density. The unipolar phase current of 180° electrical conduction period has the highest efficiency and the lowest torque ripple. For double layer short pitched winding, sinusoidal current excitation has the maximum torque density and the minimum torque ripple.

Modeling methods for MCSRMs have also been discussed. Analytical modeling methods are the inductance model and the equivalent magnetic circuit model. Inductance models show accurate results in modeling the self inductance, while they might not be accurate enough to model the mutual coupling, since that requires large number of experiments or FEA simulations. The equivalent magnetic circuit model can be used to model the mutual coupling in CSRM, where the mutual inductance is assumed to be dependent on rotor position only. Equivalent magnetic circuit model can also be used for MCSRMs for 2-phase excitation, where the two excited phases have equal current without phase shift. LUT based modeling methods are the most accurate way to model mutual coupling. A detailed explanation of this method is presented including the inversion of the LUTs obtained from FEA.

MCSRMs combine the advantages of CSRM, which has a simple and robust structure, with the advantages of AC motors, which enable the use of standard motor drives. Improving the MCSRM performance through the optimization of the dq currents and by the mitigation of spatial harmonics are the future trends for sinusoidal excitation. Current profile shaping and distributed winding configurations can improve the motor performance and they have not been investigated in the literature, yet.

ACKNOWLEDGMENT

The authors gratefully acknowledge Powersys Solutions for their support with JMAG software in this research.

REFERENCES

[1] M. Ehsani, J. T. Bass, T. J. E. Miller, and R. L. Steigerwald, "Development of a unipolar converter for variable reluctance motor drives," *IEEE Trans. Ind. Appl.*, vols. IA–23, no. 3, pp. 545–553, May 1987.

[2] M. Barnes and C. Pollock, "Power electronic converters for switched reluctance drives," *IEEE Trans. Power Electron.*, vol. 13, no. 6, pp. 1100–1111, Nov. 1998.

[3] P. J. Lawrenson, J. M. Stephenson, P. T. Blenkinsop, J. Corda, and N. N. Fulton, "Variable-speed switched reluctance motors," *IEE Proc. B-Electr. Power Appl.*, vol. 127, no. 4, pp. 253–265, Jul. 1980.

[4] W. F. Ray and R. M. Davis, "Inverter drive for doubly salient reluctance motor: Its fundamental behaviour, linear analysis and cost implications," *IEE J. Electr. Power Appl.*, vol. 2, no. 6, pp. 185–193, Dec. 1979.

[5] B. Bilgin, J. W. Jiang, and A. Emadi, "Electromagnetic principles in switched reluctance motors," in *Switched Reluctance Motor Drives: Fundamentals to Applications*. Boca Raton, FL, USA: CRC Press, 2019.

[6] A. V. Radun, "Design considerations for the switched reluctance motor," *IEEE Trans. Ind. Appl.*, vol. 31, no. 5, pp. 1079–1087, Sep. 1995.

[7] B. C. Mecrow, "Fully pitched-winding switched-reluctance and stepping-motor arrangements," *IEE Proc. B, Electr. Power Appl.*, vol. 140, no. 1, pp. 61–70, Jan. 1993.

[8] B. C. Mecrow, "New winding configurations for doubly salient reluctance machines," *IEEE Trans. Ind. Appl.*, vol. 32, no. 6, pp. 1348–1356, Nov. 1996.

[9] Y. Xu and D. A. Torrey, "Study of the mutually coupled switched reluctance machine using the finite element-circuit coupled method," *IEE Proc. Electr. Power Appl.*, vol. 149, no. 2, pp. 81–86, Mar. 2002.

[10] M. A. Kabir and I. Husain, "Design of mutually coupled switched reluctance motors (MCSRMs) for extended speed applications using 3-phase standard inverters," *IEEE Trans. Energy Convers.*, vol. 31, no. 2, pp. 436–445, Jun. 2016.

[11] C. S. Edrington, M. Krishnamurthy, and B. Fahimi, "Bipolar switched reluctance machines: A novel solution for automotive applications," *IEEE Trans. Veh. Technol.*, vol. 54, no. 3, pp. 795–808, May 2005.

[12] X. B. Liang, G. J. Li, J. Ojeda, M. Gabsi, and Z. Ren, "Comparative study of vibration and acoustic noise between classical and mutually coupled switched reluctance motors," in *Proc. 11th Int. Conf. Elect. Mach.*, Marseille, France, Sep. 2012, pp. 2955–2960.

[13] X. Liang, G. Li, J. Ojeda, M. Gabsi, and Z. Ren, "Comparative study of classical and mutually coupled switched reluctance motors using multiphysics finite-element modeling," *IEEE Trans. Ind. Electron.*, vol. 61, no. 9, pp. 5066–5074, Sep. 2014.

[14] V. P. Vujičić, "Minimization of torque ripple and copper losses in switched reluctance drive," *IEEE Trans. Power Electron.*, vol. 27, no. 1, pp. 388–399, Jan. 2012.

[15] P. L. Chapman and S. D. Sudhoff, "Design and precise realization of optimized current waveforms for an 8/6 switched reluctance drive," *IEEE Trans. Power Electron.*, vol. 17, no. 1, pp. 76–83, Jan. 2002.

[16] A. D. Callegaro, B. Bilgin, and A. Emadi, "Radial force shaping for acoustic noise reduction in switched reluctance machines," *IEEE Trans. Power Electron.*, vol. 34, no. 10, pp. 9866–9878, Oct. 2019.

[17] H. Li, B. Bilgin, and A. Emadi, "An improved torque sharing function for torque ripple reduction in switched reluctance machines," *IEEE Trans. Power Electron.*, vol. 34, no. 2, pp. 1635–1644, Feb. 2019.

[18] G. J. Li, X. Y. Ma, G. W. Jewell, Z. Q. Zhu, and P. L. Xu, "Influence of conduction angles on single-layer switched reluctance machines," *IEEE Trans. Mag.*, vol. 52, no. 12, pp. 1–11, Dec. 2016.

[19] X. Y. Ma, G. J. Li, G. W. Jewell, Z. Q. Zhu, and H. L. Zhan, "Performance comparison of doubly salient reluctance machine topologies supplied by sinewave currents," *IEEE Trans. Ind. Electron.*, vol. 63, no. 7, pp. 4086–4096, Jul. 2016.

[20] C. Gan, J. Wu, Q. Sun, W. Kong, H. Li, and Y. Hu, "A review on machine topologies and control techniques for low-noise switched reluctance motors in electric vehicle applications," *IEEE Access*, vol. 6, pp. 31430–31443, May 2018.

[21] K. Vijayakumar, R. Karthikeyan, S. Paramasivam, R. Arumugam, and K. N. Srinivas, "Switched reluctance motor modeling, design, simulation, and analysis: A comprehensive review," *IEEE Trans. Magn.*, vol. 44, no. 12, pp. 4605–4617, Dec. 2008.

[22] S. D. Sudhoff and P. C. Krause, "Analysis of steady-state operation of a multistack variable-reluctance stepper motor using qdO variables," *IEEE Trans. Energy Convers.*, vol. 6, no. 4, pp. 693–699, Dec. 1991.

[23] J. Bernat, J. Kolota, and S. Stepien, "Proportional-integral-derivative position control of variable reluctance stepper motor," in *Proc. Int. Symp. Theor. Eng.*, Lübeck, Germany, Jun. 2009, pp. 1–4.

[24] J. W. Finch, H. M. B. Metwally, and J. A. Agber, "Performance prediction in saturated variable reluctance and hybrid motors," in *Proc. 4th Int. Conf. Power Electron. Variable-Speed Drives*, Jul. 1990, pp. 231–236.

[25] J. W. Finch, "Design method for torque estimation in stepping and switched reluctance motors," in *Proc. IEEE Colloq. Stepper Motors Control*, Jan. 1994, pp. 3/1–3/3.

[26] G. J. Li, Z. Q. Zhu, X. Y. Ma, and G. W. Jewell, "Comparative study of torque production in conventional and mutually coupled SRMs using frozen permeability," *IEEE Trans. Magn.*, vol. 52, no. 6, Jun. 2016, Art. no. 8103509.

[27] G. J. Li, K. Zhang, Z. Q. Zhu, and G. W. Jewell, "Comparative studies of torque performance improvement for different doubly salient synchronous reluctance machines by current harmonic injection," *IEEE Trans. Energy Convers.*, vol. 34, no. 2, pp. 1094–1104, Jun. 2019.

[28] J.-W. Ahn, S.-G. Oh, J.-W. Moon, and Y.-M. Hwang, "A three-phase switched reluctance motor with two-phase excitation," *IEEE Trans. Ind. Appl.*, vol. 35, no. 5, pp. 1067–1075, Sep. 1999.

[29] G. J. Li, J. Ojeda, E. Hoang, M. Lecrivain, and M. Gabsi, "Comparative studies between classical and mutually coupled switched reluctance motors using thermal-electromagnetic analysis for driving cycles," *IEEE Trans. Magn.*, vol. 47, no. 4, pp. 839–847, Apr. 2011.

[30] J. M. Kokernak and D. A. Torrey, "Magnetic circuit model for the mutually coupled switched-reluctance machine," *IEEE Trans. Magn.*, vol. 36, no. 2, pp. 500–507, Mar. 2000.

[31] W. Uddin and Y. Sozer, "Analytical modeling of mutually coupled switched reluctance machines under saturation based on design geometry," *IEEE Trans. Ind. Appl.*, vol. 53, no. 5, pp. 4431–4440, Sep. 2017.

[32] B. C. Mecrow, C. Weiner, and A. C. Clothier, "The modeling of switched reluctance machines with magnetically coupled windings," *IEEE Trans. Ind. Appl.*, vol. 37, no. 6, pp. 1675–1683, Nov. 2001.

[33] Y. Li and Y. Tang, "Switched reluctance motor drives with fractionally-pitched winding design," in *Proc. 28th Annu. IEEE Power Electron. Spec. Conf. Formerly Power Conditioning Spec. Conf. Power Process. Electron. Spec. Conf.*, Saint Louis, MO, USA, Jun. 1997, pp. 875–880.

[34] B. Howey, "Non-coupled and mutually coupled switched reluctance machines for an e-bike traction application: Pole configurations, design, and comparison," Ph.D. dissertation, Dept. Mech. Eng., McMaster Univ., Hamilton, ON, Canada, Aug. 2018.

[35] X. Liu, Z. Q. Zhu, M. Hasegawa, A. Pride, R. Deodhar, T. Maruyama, and Z. Chen, "Performance comparison between unipolar and bipolar excitations in switched reluctance machine with sinusoidal and rectangular waveforms," in *Proc. IEEE Energy Convers. Congr. Expo.*, Phoenix, AZ, USA, Sep. 2011, pp. 1590–1595.

[36] P. Krause, O. Wasynczuk, S. D. Sudhoff, and S. Pekarek, "Synchronous machines," in *Analysis of Electric Machinery and Drive Systems*, 3rd ed. Hoboken, NJ, USA, Wiley, 2013.

[37] A. C. Clothier, "Switched reluctance motor drives with fully pitched windings," Ph.D. dissertation, Dept. Elect. Electron. Eng., Newcastle Univ., Newcastle, U.K., Sep. 2001.

[38] M. A. Kabir and I. Husain, "Hybrid excitation topologies for three-phase mutually coupled reluctance machine with standard inverters," in *Proc. IEEE Power Energy Soc. Gen. Meeting*, Denver, CO, USA, Jul. 2015, pp. 1–5.

[39] G. J. Li, X. Ojeda, S. Hlioui, E. Hoang, M. Gabsi, and C. Balpe, "Comparative study of switched reluctance motors performances for two current distributions and excitation modes," in *Proc. 35th Annu. Conf. IEEE Ind. Electron.*, Porto, Portugal, Nov. 2009, pp. 4047–4052.

[40] M. Mohseni and S. M. Islam, "A new vector-based hysteresis current control scheme for three-phase PWM voltage-source inverters," *IEEE Trans. Power Electron.*, vol. 25, no. 9, pp. 2299–2309, Sep. 2010.

[41] A. Tilli and A. Tonielli, "Sequential design of hysteresis current controller for three-phase inverter," *IEEE Trans. Ind. Electron.*, vol. 45, no. 5, pp. 771–781, Oct. 1998.

[42] B.-H. Kwon, B.-D. Min, and J.-H. Youm, "An improved space-vector-based hysteresis current controller," *IEEE Trans. Ind. Electron.*, vol. 45, no. 5, pp. 752–760, Oct. 1998.

[43] Y. Chen and K. M. Smedley, "A cost-effective single-stage inverter with maximum power point tracking," *IEEE Trans. Power Electron.*, vol. 19, no. 5, pp. 1289–1294, Sep. 2004.

[44] A. M. Michaelides and C. Pollock, "Modelling and design of switched reluctance motors with two phases simultaneously excited," *IEE Proc. Electr. Power Appl.*, vol. 143, no. 5, pp. 361–370, Sep. 1996.

[45] T. Husain, W. Uddin, and Y. Sozer, "Performance comparison of short-pitched and fully pitched switched reluctance machines over wide speed operations," *IEEE Trans. Ind. Appl.*, vol. 54, no. 5, pp. 4278–4287, Sep./Oct. 2018.

[46] C. Ma, L. Qu, and Z. Tang, "Torque ripple reduction for mutually coupled switched reluctance motor by bipolar excitations," in *Proc. Int. Electr. Mach. Drives Conf.*, May 2013, pp. 1211–1217.

[47] C. Ma and L. Qu, "Design considerations of switched reluctance motors with bipolar excitation for low torque ripple applications," in *Proc. IEEE Energy Convers. Congr. Expo.*, Sep. 2013, pp. 926–933.

[48] J. Park, S. Jung, and J.-I. Ha, "Variable time step control for six-step operation in surface-mounted permanent magnet machine drives," *IEEE Trans. Power Electron.*, vol. 33, no. 2, pp. 1501–1513, Feb. 2018.

[49] Y.-C. Kwon, S. Kim, and S.-K. Sul, "Six-step operation of PMSM with instantaneous current control," *IEEE Trans. Ind. Appl.*, vol. 50, no. 4, pp. 2614–2625, Jul./Aug. 2014.

[50] P. Chancharoensook and M. F. Rahman, "Dynamic modeling of a four-phase 8/6 switched reluctance motor using current and torque look-up tables," in *Proc. 28th Annu. Conf. Ind. Electron. Soc.*, Seville, Spain, Nov. 2002, pp. 491–496.

[51] C. S. Edrington, B. Fahimi, and M. Krishnamurthy, "An autocalibrating inductance model for switched reluctance motor drives," *IEEE Trans. Ind. Electron.*, vol. 54, no. 4, pp. 2165–2173, Aug. 2007.

[52] M. Krishnamurthy, B. Fahimi, and C. S. Edrington, "On the measurement of mutual inductance for a switched reluctance machine," in *Proc. 37th IEEE Power Electron. Spec. Conf.*, Jeju, South Korea, Jun. 2006, pp. 1–7.

[53] X. Ding, M. Rashed, C. I. Hill, and S. Bozhko, "Analytical modelling approach for switched reluctance machines with deep saturation," in *Proc. Int. Conf. Elect. Syst. Aircr., Railway, Ship Propuls. Road Vehicles Int. Transp. Electrific. Conf.*, Toulouse, France, Nov. 2016, pp. 1–6.

[54] H. Gao, F. R. Salmasi, and M. Ehsani, "Inductance model-based sensorless control of the switched reluctance motor drive at low speed," *IEEE Trans. Power Electron.*, vol. 19, no. 6, pp. 1568–1573, Nov. 2004.

[55] J. Mahdavi, G. Suresh, B. Fahimi, and M. Ehsani, "Dynamic modeling of nonlinear SRM drive with Pspice," in *Proc. IEEE Ind. Appl. Conf. 32nd IAS Annu. Meeting*, New Orleans, LA, USA, Oct. 1997, pp. 661–667.

[56] B. Fahimi, G. Suresh, J. Mahdavi, and M. Ehsani, "A new approach to model switched reluctance motor drive application to dynamic performance prediction, control and design," in *Proc. 29th Annu. IEEE Power Electron. Spec. Conf.*, Fukuoka, Japan, May 1998, pp. 2097–2102.

[57] F. R. Salmasi and M. Ehsani, "A novel approach to auto-calibrating sensorless switched reluctance motor drive," in *Proc. 29th Annu. Conf. IEEE Ind. Electron. Soc.*, Roanoke, VA, USA, Nov. 2003, pp. 2471–2476.

[58] X. Zhang, F. Wang, and X. Wu, "Low-speed direct-driven sensorless control including zero-speed for switched reluctance motor based on dynamic inductance model," in *Proc. 17th Int. Conf. Elect. Mach. Syst. (ICEMS)*, Oct. 2014, pp. 763–767.

[59] S. Kuai, V. Rallabandi, and D. M. Ionel, "Sensorless control of three phase switched reluctance motor drives using an approximate inductance model," in *Proc. IEEE Int. Electr. Mach. Drives Conf. (IEMDC)*, Miami, FL, USA, May 2017, pp. 1–6.

[60] A. Nirgude, M. Murali, N. Chaithanya, S. Kulkarni, V. B. Bhole, and S. R. Patel, "Nonlinear mathematical modeling and simulation of switched reluctance motor," in *Proc. IEEE Int. Conf. Power Electron. Drives Energy Syst. (PEDES)*, Trivandrum, India, Dec. 2016, pp. 1–6.

[61] C. S. Edrington and B. Fahimi, "An auto-calibrating model for an 8/6 switched reluctance motor drive: Application to design and control," in *Proc. 34th Annu. Conf. Power Electron. Spec.*, Acapulco, Mexico, Jun. 2003, pp. 409–415.

[62] S. S. Ramamurthy, R. M. Schupbach, and J. C. Balda, "Artificial neural networks based models for the multiply excited switched reluctance motor," in *Proc. 16th Annu. IEEE Appl. Power Electron. Conf. Expo.*, Anaheim, CA, USA, vol. 2, Mar. 2001, pp. 1109–1115.

[63] M. Preston and J. P. Lyons, "A switched reluctance motor model with mutual coupling and multi-phase excitation," *IEEE Trans. Magn.*, vol. 27, no. 6, pp. 5423–5425, Nov. 1991.

[64] V. Vujicic and S. N. Vukosavic, "A simple nonlinear model of the switched reluctance motor," *IEEE Trans. Energy Convers.*, vol. 15, no. 4, pp. 395–400, Dec. 2000.

[65] D. S. Mihic, M. V. Terzic, and S. N. Vukosavic, "A new nonlinear analytical model of the SRM with included multiphase coupling," *IEEE Trans. Energy Convers.*, vol. 32, no. 4, pp. 1322–1334, Dec. 2017.

[66] H.-K. Bae, "Control of switched reluctance motors considering mutual inductance," Ph.D. dissertation, Bradley Dept. Elect. Comput. Eng., Virginia Polytech. Inst. State Univ., Blacksburg, VA, USA, Aug. 2000.

[67] D. N. Essah and S. D. Sudhoff, "An improved analytical model for the switched reluctance motor," *IEEE Trans. Energy Convers.*, vol. 18, no. 3, pp. 349–356, Sep. 2003.

[68] M. Boesing, M. Niessen, T. Lange, and R. D. Doncker, "Modeling spatial harmonics and switching frequencies in PM synchronous machines and their electromagnetic forces," in *Proc. 11th Int. Conf. Elect. Mach.*, Marseille, France, Sep. 2012, pp. 3001–3007.

[69] J. Dong, B. Howey, B. Danen, J. Lin, J. W. Jiang, B. Bilgin, and A. Emadi, "Advanced dynamic modeling of three-phase mutually coupled switched reluctance machine," *IEEE Trans. Energy Convers.*, vol. 33, no. 1, pp. 146–154, Mar. 2018.

[70] J. D'Errico. (2006). *Understanding Gridfit*. Accessed: Mar. 2016. [Online]. Available: http://www.mathworks.com/matlabcentral/fileexchange/8998

[71] A. K. Jain and N. Mohan, "Dynamic modeling, experimental characterization, and verification for SRM operation with simultaneous two-phase excitation," *IEEE Trans. Ind. Electron.*, vol. 53, no. 4, pp. 1238–1249, Jun. 2006.

[72] W. Uddin and Y. Sozer, "Modeling of mutually coupled switched reluctance motors for torque ripple minimization," in *Proc. IEEE Int. Electr. Mach. Drives Conf. (IEMDC)*, Coeur d'Alene, ID, USA, May 2015, pp. 1006–1010.

[73] M. Karacor, K. Yilmaz, and F. E. Kuyumcu, "Modeling MCSRM with artificial neural network," in *Proc. Int. Aegean Conf. Elect. Mach. Power Electron.*, Sep. 2007, pp. 849–852.

[74] S. Mehta, A. Kabir, and I. Husain, "Decoupled modeling of mutually coupled SRM based on net flux method," in *Proc. IEEE Transp. Electrific. Conf. Expo (ITEC)*, Long Beach, CA, USA, Jun. 2018, pp. 114–118.

[75] W. Ding, D. Liang, and H. Sui, "Dynamic modeling and performance prediction for dual-channel switched reluctance machine considering mutual coupling," *IEEE Trans. Magn.*, vol. 46, no. 9, pp. 3652–3663, Sep. 2010.

[76] W. Ding, J. Lou, and L. Liu, "Improved decoupled model of mutually coupled dual-channel SRM with consideration of magnetic saturation in dual-channel operation," *IET Electr. Power Appl.*, vol. 7, no. 6, pp. 427–440, Jul. 2013.

[77] (Aug. 2014). *JMAG-RT|JMAG Simulation Technology for Electromechanical Design*. Accessed: Jul. 6, 2019. [Online]. Available: https://powersys-solutions.com/2016/10/03/utilizing-saber-with-jmag/

[78] (Oct. 2016). *Utilizing SABER With JMAG*. accessed: Jul. 6, 2019. [Online]. Available: https://powersys-solutions.com/2016/10/03/utilizing-saber-with-jmag/

[79] (Sep. 2010). *MATLAB Third-Party Products & Services*. Accessed: Jul. 6, 2019. [Online]. Available: https://www.mathworks.com/products/connections/product_detail/jmag.html

PETER AZER (S'19) received the bachelor's and master's degrees in electrical engineering from Ain Shams University, Cairo, Egypt, in 2013 and 2016, respectively. He is currently pursuing the Ph.D. degree in electrical and computer engineering with McMaster University, Hamilton, ON, Canada. His areas of research includes power electronics, motor drives, switched reluctance machines (SRM), fault-tolerant control, and system modeling.

BERKER BILGIN (S'09–M'11–SM'16) received the Ph.D. degree in electrical engineering from the Illinois Institute of Technology in Chicago, Illinois, USA, and the MBA degree from DeGroote School of Business, McMaster University, Hamilton, ON, Canada. He is currently an Assistant Professor with the Department of Electrical and Computer Engineering (ECE), McMaster University. Before joining the ECE department, he was the Chief Engineer and the Research Program Manager with the Canada Excellence Research Chair in Hybrid Powertrain Program at the McMaster Institute for Automotive Research and Technology (MacAUTO). His research interests include electric machines, switched reluctance motor drives, acoustic noise and vibration analysis and reduction, and power electronics and electric motor drives. He is the Lead Editor and the author of the textbook titled *Switched Reluctance Motor Drives: Fundamentals to Applications*. He is the principal author/coauthor of 81 journals and conference papers and three book chapters. He is the principal inventor/co-inventor of 10 patents and pending patent applications. He is the Co-Founder and the VP of engineering of Enedym Inc., which is a spin-off company of McMaster University. Enedym specializes in electric machines, electric motor drives, advanced controls and software, and virtual engineering. He was the General Chair of the 2016 IEEE Transportation Electrification Conference and Expo (ITEC). He is also an Associate Editor of the IEEE TRANSACTIONS ON TRANSPORTATION ELECTRIFICATION.

ALI EMADI (S'98–M'00–SM'03–F'13) received the B.S. and M.S. degrees (Hons.) in electrical engineering from the Sharif University of Technology, Tehran, Iran, in 1995 and 1997, respectively, and the Ph.D. degree in electrical engineering from Texas A&M University, College Station, TX, USA, in 2000. He is the Canada Excellence Research Chair Laureate with McMaster University, Hamilton, Ontario, Canada. He is also the Holder of the NSERC/FCA Industrial Research Chair in Electrified Powertrains and Tier I Canada Research Chair in Transportation Electrification and Smart Mobility. Before joining McMaster University, he was the Harris Perlstein Endowed Chair Professor of Engineering and the Director of the Electric Power and Power Electronics Center and Grainger Laboratories, Illinois Institute of Technology, Chicago, where he established research and teaching facilities as well as courses in power electronics, motor drives, and vehicular power systems. He was the Founder, Chairman, and the President of the Hybrid Electric Vehicle Technologies, Inc. (HEVT) — a university spin-off company of Illinois Tech. He has been a recipient of numerous awards and recognitions. He was the Advisor for the Formula Hybrid Teams at Illinois Tech and McMaster University, which won the GM Best Engineered Hybrid System Award at the 2010, 2013, and 2015 competitions. He is the principal author/coauthor of over 450 journals and conference papers as well as several books, including the *Vehicular Electric Power Systems* (2003), the *Energy Efficient Electric Motors* (2004), the *Uninterruptible Power Supplies and Active Filters* (2004), the *Modern Electric, Hybrid Electric, and Fuel Cell Vehicles* (2nd ed., 2009), and the *Integrated Power Electronic Converters and Digital Control* (2009). He is also the Editor of the *Handbook of Automotive Power Electronics and Motor Drives* (2005) and the *Advanced Electric Drive Vehicles* (2014). He is the Co-Editor of the *Switched Reluctance Motor Drives* (2018). He was the Inaugural General Chair of the 2012 IEEE Transportation Electrification Conference and Expo (ITEC) and has chaired several IEEE and SAE conferences in the areas of vehicle power and propulsion. He is the founding Editor-in-Chief of the IEEE TRANSACTIONS ON TRANSPORTATION ELECTRIFICATION.